

Low-Speed Sensorless Control for Wind Turbine System

MOHAMMED TAOUSSI⁽¹⁾, MOHAMMED KARIM⁽¹⁾, BADRE BOSSOUFI⁽²⁾, DALILA HAMMOUMI⁽¹⁾, CHAKIB EL BAKKALI⁽¹⁾, AZIZ DEROUICH⁽³⁾, NAJIB EL OUANJLI⁽³⁾

⁽¹⁾Laboratory of Systems Integration and Advanced Technologies (LISTA), Faculty of Sciences Dhar El Mahraz, University Sidi Mohammed Ben Abdellah Fez - MAROCCO

m.taoussi0@gmail.com

⁽²⁾Laboratory of Electrical Engineering and Maintenance (LGEM) ESTO School of Technology, University Mohammed I Oujda - MAROCCO

⁽³⁾Laboratory Production Engineering, Energy and Sustainable Development (PE2D), College of Technology, University Sidi Mohammed Ben Abdellah Fez - MAROCCO

Abstract: - In the propose of the work, we concerns the elaboration an efficient and robust control of active and reactive power by the use the PI regulators control (FOC) a power converters directly connected to the stator and the rotor of a Doubly Fed Induction Generator (DFIG) system incorporated in a wind turbine to improve the performance of a speed wind turbine. In the aim to assess the performance and dynamics of the wind system, for the different test speeds of the wind, we are interested in the modeling, development and control of the wind system. Initially, a control strategy of the MPPT-DFIG is presented. Therefore, the aim is the study and implementation of the new control technique for wind systems. This control technique is based on the orientation control of the flow rotor to DFIG. Finally, the control simulation results are simulated on the environment Matlab / Simulink. A very detailed analysis of simulation results of wind conversion chain system is performed with the objective to evaluate and optimize the performance of the proposed system.

Key-Words: - Wind Turbine; DFIG-Generator; modeling; Rotor Control; vector control; MPPT Control; Orientation of the flow rotorique; Matlab / Simulink.

1 Introduction

The electricity has become more and more essential for humanity. Indeed, access to electricity, is the guarantee of best living conditions (hygiene, health, education). So it is at the heart about the future of our society. It is as much by a factor of construction and wealth creation. On the one hand, demographic evolution of the world implies a sustainable increase in energy needs. Moreover, energy consumption, still on the increase, is reduce fossil energy reserves (coal, oil, gas) and away from the use of polluting fossil energy (carbon dioxide emissions), many countries have looked to renewable energy. There are many renewable energy resources: hydropower, wind power, solar thermal and photovoltaic, the energy produced by the waves and marine currents, geothermal and biomass [1]. These energy resources are virtually inexhaustible and clean. The wind power is among the renewable energies, the one that knows the fastest growing in the world. It is almost universally recognized as the most promising source of energy to produce clean electricity in the short and medium term. And it contributes to environmental preservation.

Currently, Sustainable development and renewable energy today arouse the interest of

several research teams. Thus, the development and the multiplication of wind turbines have led the researchers to improve the efficiency of electromechanical conversion and quality of the energy supplied. It is in this context that we present a study on the use of a doubly fed induction generator (DFIG) in a wind system, because of the many advantages over other types of electric machines, since its construction is simple, its low cost, its security interest of operation, its robustness and especially its simple and economical maintenance. Through evolution and development of new technology recent power electronics and informatics, the problems inherent in the controls and operation of the various applications of the speed variables DFIG are resolved and simplified.

In this context, for appropriate operation of the variable speed DFIG, one must insert a power converter PWM and control by vector control orientation of the flow rotor, whose objective is to regulate the electrical power extract it from the machine to its reference value, we apply this control to successfully DFIG, which gave a good powerful tool for its control. The performance of this control will be conducted by simulation results with interpretations. Figure 1 presents a general structure

of the electrical control of the wind energy system, which is studied in this work, constituted the wind turbine with three swivel blade length R, the DFIG generator and the speed multiplier:

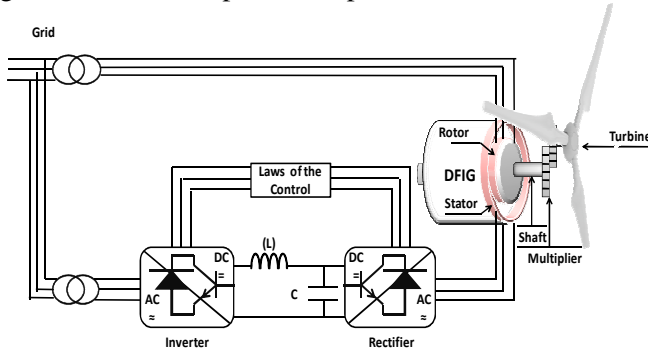


Figure 1. Overall architecture of the control system of the wind.

2 Modeling of Wind Power System

2.1 Modeling of the Turbine

The modeling of the wind turbine is characterized by the curves of the power coefficient, which corresponds to the relation between the mechanical power extract from the wind and the incident power. The expression for the power extracted available on the rotor of the turbine, is expressed by [2]:

$$\begin{cases} P_{\text{Extrait}} = P_{\text{Incident}} \cdot C_p(\lambda, \beta) \\ P_{\text{Incident}} = \frac{1}{2} \rho \cdot S \cdot v^3 \end{cases} \quad (1)$$

With:

S: The surface swept by the blades of the turbine (m²).

ρ : The density of air ($\rho = 1.225 \text{ kg/m}^3$).

V : Wind speed (m/s).

$C_p(\lambda, \beta)$: Power coefficient.

Hence the power coefficient, $C_p(\lambda, \beta)$, to a limit known as Betz limit. This limit is the maximum extractable power for a given wind speed $C_p^{\text{max}}(\lambda, \beta) \approx 0.593$ [15]. For the DFIG, the power coefficient is possible to model with a single equation that depends on the speed ratio λ and the orientation angle $\hat{\alpha}$ of the blades as follows [2]:

$$C_p(\lambda, \beta) = c_1 \cdot \left(c_2 \cdot \frac{1}{A} - c_3 \cdot \beta - c_4 \right) e^{-c_5 \frac{1}{A}} + c_6 \cdot \lambda \quad (2)$$

With:

$$\begin{cases} c_1 = 0.5872 \\ c_2 = 116 \\ c_3 = 0.4 \\ c_4 = 5 \\ c_5 = 21 \\ c_6 = 0.0085 \end{cases} \quad \text{et} \quad \begin{cases} \frac{1}{A} = \frac{1}{\lambda + 0.08 \cdot \beta} - \frac{0.035}{1 + \beta^3} \\ \lambda = \frac{\Omega_t \cdot R}{v} \end{cases} \quad (3)$$

From equation (2), it displays the power coefficient curves as a function of λ for different β values [23]:

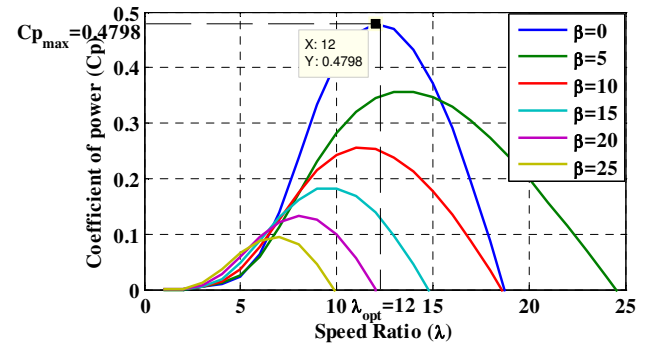


Figure 2. Curves of the Cp power coefficient as a function of λ and β .

From Figure 2, we obtain a maximum power coefficient $C_p^{\text{max}}(\lambda, \beta) = 0.4798$, for a speed ratio $\lambda = 12$ and $\beta = 0$, by setting λ_{opt} and β respectively to their optimal values; the wind system will provide optimal electrical power. The power and mechanical torque of the turbine is noted [8]:

$$P_{\text{mec}} = \frac{1}{2} \rho \cdot S \cdot C_p(\lambda, \beta) \cdot v^3 \quad (4)$$

$$C_{\text{mec}} = \frac{P_{\text{mec}}}{\Omega_t} = \frac{1}{2} \rho \cdot S \cdot C_p(\lambda, \beta) \cdot v^3 \cdot \frac{1}{\Omega_t}$$

With:

Ω_t : The turbine rotation speed.

C_{mec} : Torque on the slow axis (turbine side).

According to equations (1), (2), (3) and (4), we model the turbine as follows:

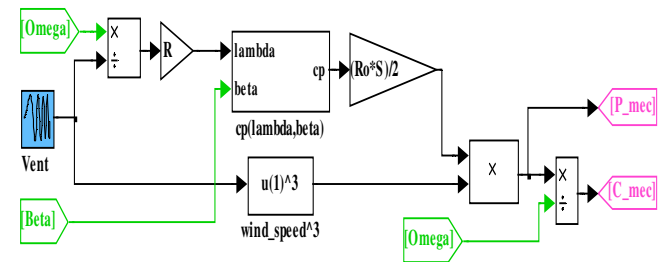


Figure 3. Modeling of the wind turbine.

2.2 Multiplier modeling

The multiplier is the connection between the wind turbine and DFIG. It is adapted the speed of the turbine to that of the generator as well mechanical torque on the shaft of the generator by the following equations [3]:

$$\Omega_g = \frac{1}{G} \Omega_t \tag{5}$$

$$C_{aer} = \frac{1}{G} C_g$$

With:

Ω_g : generator speed (speed shaft in rad/s).

G: multiplication ratio.

Ω_t : blade rotation speed (output shaft in rad/s).

C_g : mechanical torque on the axis of the generator (Nm).

C_{aer} : mechanical turbine torque (N · m).

The next block diagram represents the modeling of the multiplier for wind:

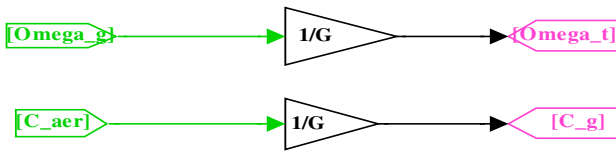


Figure 4. Modeling of wind multiplier.

2.3 Shaft Modeling

The fundamental equation of the dynamics that characterize the mechanical behavior of the turbine and generator from the total mechanical torque (C_{mec}) applied to the rotor is given by the following formula:

$$J \frac{d\Omega_{mec}}{dt} = C_{mec}$$

$$C_{mec} = C_{ar} - C_{em} - C_{vis} \tag{6}$$

$$C_{vis} = f \cdot \Omega_{mec}$$

With:

Ω_{mec} : Mechanical speed the DFIG.

C_{ar} : Aerodynamic torque on the fast axis of the turbine.

C_{em} : Electromagnetic torque.

f : friction coefficient.

In operation the electromagnetic torque generator C_{mec} has a negative sign. The next block diagram represents the modeling of the shaft for wind [10]:

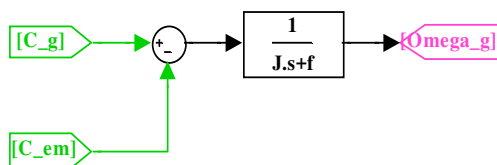


Figure 5. Modeling of the turbine shaft.

3 Extraction of Maximum Power by the Method MPPT

The MPPT (Maximum Power Point Tracking) is a principle for tracking the maximum power point of an electric generator for a variant source. The MPPT has been created to have the best possible connection between the source and the nonlinear grid to extract the maximum power.

In order to capture the maximum power of the incident wind, must permanently adjust the rotation speed of the turbine to the wind. The wind speed is difficult to measure, we assume that the wind speed is constant over the study period, the rotation speed of the turbine is assumed to be constant with respect to the high inertia of the latter. If we neglect the friction coefficient of the mechanical shaft, we can write the following equation [4]:

$$C_g = C_{em} \tag{7}$$

With, C_g is the torque exerted on the shaft after the multiplier.

Then, the reference of the electromagnetic torque of the turbine is obtained from the following equation:

$$\begin{cases} C_{em_ref} = \frac{C_{aer}}{G} \\ C_{aer} = \frac{1}{2 \cdot \Omega_t} C_{p_max} \cdot \rho \cdot V^3 \\ V = \frac{R \cdot \Omega_t}{\lambda_{opt}} \end{cases} \tag{8}$$

Hence the electromagnetic torque reference is:

$$C_{em_ref} = \frac{1}{2 \cdot \lambda_{opt} \cdot G^3} C_{p_max} \cdot \rho \cdot \pi^2 \cdot \Omega^2 \tag{9}$$

The following block diagram shows the extraction modeling of the maximum power from the equation (9):

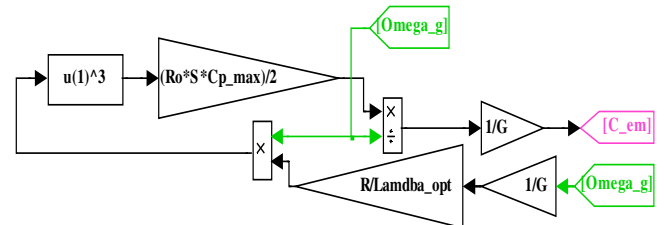


Figure 6. Maximum power extraction model by startigé MPPT.

On the basis of the previous equations and models, the global schema we can give to all the dynamic model of the wind turbine (Fig 7):

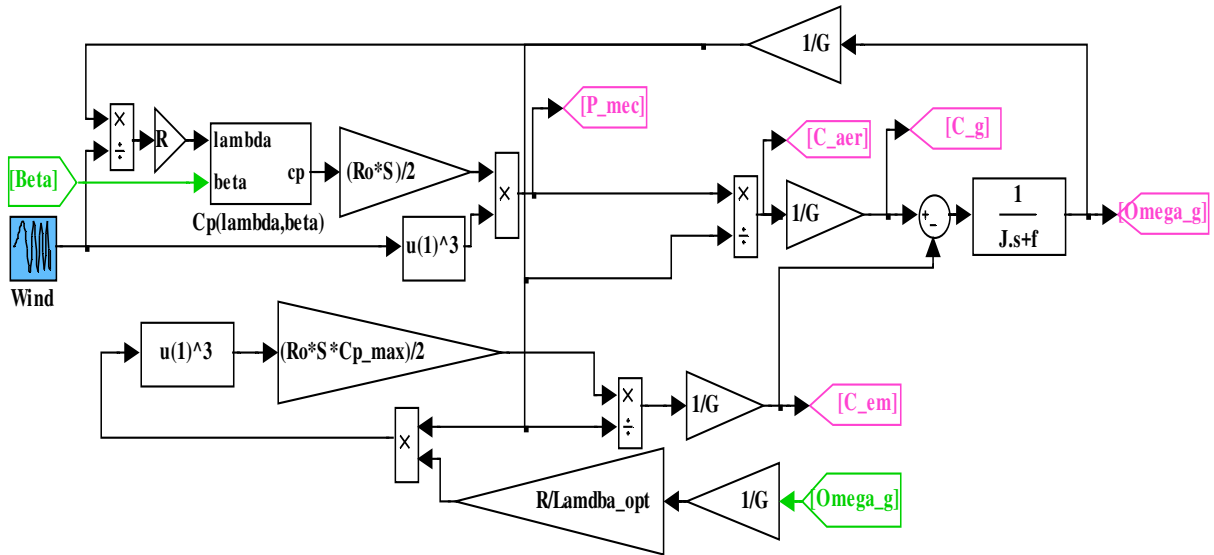


Figure 7. Synoptic diagram of global model the wind turbine with maximum power extraction.

4 Modeling of the DFIG

For a better representation of the behavior of a doubly fed induction generator, it is necessary to use a specific model and simple. The two-phase models (d, q) given by the Park transformation is used [9].

4.1 Electrical Equations of DFIG

The equations of the stator voltages $V_s(d, q)$ and the rotor $V_r(d, q)$, the dynamic model are expressed by DFIG [5]:

$$\begin{cases} V_{sd} = R_s \cdot I_{sd} + \frac{d\varphi_{sd}}{dt} - \omega_s \cdot \varphi_{sq} \\ V_{sq} = R_s \cdot I_{sq} + \frac{d\varphi_{sq}}{dt} + \omega_s \cdot \varphi_{sd} \\ V_{rd} = R_r \cdot I_{rd} + \frac{d\varphi_{rd}}{dt} - \omega_r \cdot \varphi_{rq} \\ V_{rq} = R_r \cdot I_{rq} + \frac{d\varphi_{rq}}{dt} + \omega_r \cdot \varphi_{rd} \\ I_{sd} = \frac{1}{\sigma \cdot L_s} \cdot \varphi_{sd} - \frac{M_{sr}}{\sigma \cdot L_r} \cdot \varphi_{sd} \\ I_{sq} = \frac{1}{\sigma \cdot L_s} \cdot \varphi_{sq} - \frac{M_{sr}}{\sigma \cdot L_s \cdot L_r} \cdot \varphi_{sq} \\ I_{rd} = \frac{1}{\sigma \cdot L_r} \cdot \varphi_{rd} - \frac{M_{sr}}{\sigma \cdot L_r \cdot L_s} \cdot \varphi_{sd} \\ I_{rq} = \frac{1}{\sigma \cdot L_r} \cdot \varphi_{rq} - \frac{M_{sr}}{\sigma \cdot L_r \cdot L_s} \cdot \varphi_{sq} \end{cases} \quad (10)$$

4.2 Magnetic Equations

The following magnetic equations are taken from electrical equations (11):

$$\begin{cases} \varphi_{sd} = L_s \cdot I_{sd} + M_{sr} \cdot I_{rd} \\ \varphi_{sq} = L_s \cdot I_{sq} + M_{sr} \cdot I_{rq} \\ \varphi_{rd} = L_r \cdot I_{rd} + M_{sr} \cdot I_{sd} \\ \varphi_{rq} = L_r \cdot I_{rq} + M_{sr} \cdot I_{sq} \end{cases} \quad (12)$$

4.3 Mechanical Equations

The electromagnetic torque of the DFIG is:

$$C_{em} = P(\varphi_{rd} \cdot \varphi_{sq} - \varphi_{rq} \cdot \varphi_{sd}) \quad (13)$$

With:

$\varphi_s(d, q), \varphi_r(d, q)$: Stator and rotor two-phase flow in the reference of PARK.

$I_s(d, q), I_r(d, q)$: Stator currents and rotor in the reference of PARK.

R_s, R_r : Stator and rotor resistances.

L_s, L_r : Inductors cyclic stator and rotor.

M : Cyclic mutual inductance.

p : Number of machine pole pairs.

ω_s : Pulsations of the stator electrical quantities.

ω_r : Pulsations of the rotor electrical quantities.

5 Vector Control of DFIG by Orientation Flow Rotor

In this work we have proposed a vector control law for DFIG based on the orientation flow rotor. In this respect, it demonstrates the relations between the stator and rotor variables. These relations will allow the rotor to act on signals to control the exchange of active and reactive power between the rotor of the machine and the grid [11].

In this control, the flow rotor φ_r is oriented in the direction axis d. Thus, we can write [12]:

$$\varphi_{rd} = \varphi_r; \varphi_{rq} = 0 \quad (14)$$

The expression of the flow rotor and the stator then becomes:

$$\begin{cases} \varphi_{sd} = \frac{L_s}{M_{sr}} \varphi_{rd} - \frac{L_r}{M_{sr}} L_s \sigma I_{rd} \\ \varphi_{sq} = -\frac{L_r \cdot L_s}{M_{sr}} \cdot \sigma \cdot I_{rq} \\ \varphi_{rd} = M_{sr} \cdot I_M \\ \varphi_{rq} = 0 \end{cases} \quad (15)$$

The expression of the electromagnetic torque then becomes [16]:

$$C_{em} = P(\varphi_{rd} \cdot \varphi_{sq}) = -L_r \cdot L_s \cdot \sigma \cdot I_{rq} \cdot I_M \quad (16)$$

From the previous equation, we can derive the equations linking the rotor and stator voltages:

$$\begin{cases} V_{sd} = \frac{RL_s + RL_r}{M_{sr}} I_{rd} + \frac{L_r L_s \sigma}{M_{sr}} \frac{dI_{rd}}{dt} + \frac{\omega L_s L_r \sigma \frac{RR_r}{\omega}}{M_{sr}} I_{rq} + \frac{L_s}{M_{sr}} V_{rd} + \frac{R_s}{\omega M_{sr}} V_{rq} \\ V_{sq} = -\frac{\omega RL_s}{M_{sr}} I_{rq} + \frac{L_r L_s \sigma}{M_{sr}} \frac{dI_{rq}}{dt} - \omega \cdot \frac{L_r}{M_{sr}} L_s \sigma I_{rd} + \frac{\omega L_s}{\omega M_{sr}} V_{rq} \\ V_{rd} = \frac{M_{sr}}{L_s} \left(\frac{RL_s + RL_r}{M_{sr}} I_{rd} + \frac{L_r L_s \sigma}{M_{sr}} \frac{dI_{rd}}{dt} + \frac{\omega L_s L_r \sigma \frac{RR_r}{\omega}}{M_{sr}} I_{rq} - \frac{R_s}{\omega M_{sr}} V_{rq} + V_{sd} \right) \\ V_{rq} = \frac{\omega M_{sr}}{\omega L_s} \left(-\frac{\omega RL_s}{M_{sr}} I_{rq} + \frac{L_r L_s \sigma}{M_{sr}} \frac{dI_{rq}}{dt} + \omega \cdot \frac{L_r}{M_{sr}} L_s \sigma I_{rd} + V_{sq} \right) \end{cases} \quad (17)$$

The vector control the DFIG allows us to express the expressions of active and reactive power as followings:

$$\begin{cases} P_r = V_{rd} \cdot I_{rd} + V_{rq} \cdot I_{rq} \\ Q_r = V_{rq} \cdot I_{rd} - V_{rd} \cdot I_{rq} \end{cases} \quad (18)$$

We replace the Vrd and Vrq tensions in Pr and Qr are obtained:

$$\begin{cases} P_r = R_r I_{rd}^2 + R_r I_{rq}^2 + \omega_r \varphi_{rd} I_{rd} \\ Q_r = \omega_r \varphi_{rd} I_{rd} \end{cases} \quad (19)$$

The power Pr is proportional to the current Irq if the flow is kept constant. We can then write:

$$P_r - P_{rj} = KI_{rq} \quad (20)$$

$$Q_r = KI_{rd}$$

The variables references values are defined to control. Thus we have the rotor currents reference.

$$I_{rq}^* = \frac{P_r^*}{K} \quad (21)$$

$$I_{rd}^* = \frac{Q_r^*}{K}$$

6 Current Control

The current control ensures voltage regulation of the DC bus and control power factor of the grid side. The objective of the control is to maintain the voltage of DC bus constant while absorbing a current to be sinusoidal as possible, with the possibility of the grid side the power factor adjustment. The grid side converter is controlled such that the active power and reactive power grid side are written as follows [6]:

$$P = \frac{3}{2} U_m \cdot I_d \quad (21)$$

$$Q = -\frac{3}{2} U_m \cdot I_q$$

With, U_m : is the amplitude of the phase voltage.

Applying the mesh law, we obtain the tension of the filter is written in matrix form in the "abc" plan.

$$\begin{pmatrix} V_1 \\ V_2 \\ V_3 \end{pmatrix} = R_r \begin{pmatrix} I_1 \\ I_2 \\ I_3 \end{pmatrix} + L_r \frac{d}{dt} \begin{pmatrix} I_1 \\ I_2 \\ I_3 \end{pmatrix} + \begin{pmatrix} d_{n1} \\ d_{n2} \\ d_{n3} \end{pmatrix} \cdot V_{dc} \quad (22)$$

This gives the differential equation of continuous DC bus:

$$\frac{dV_{dc}}{dt} = \frac{1}{C_{dc}} [(2d_{n1} + d_{n2})I_1 + (d_{n1} + 2d_{n2})I_2] \quad (23)$$

With:

$$\begin{cases} C_{dc} \frac{dV_{dc}}{dt} = I_{dc} \\ I_{dc} = \sum_{m=1}^3 d_{mm} I_m \end{cases} \quad \text{et} \quad \begin{cases} I_3 = -I_1 - I_2 \\ d_{n3} = -d_{n1} - d_{n2} \end{cases}$$

The representation status of an inverter in the plan 'abc' is non-linear (variable in time). We use the PARK transformation plan "dq" to facilitate implantation and extraction of harmonics [13]:

$$\begin{pmatrix} V_d \\ V_q \end{pmatrix} = [P(\theta)] \begin{pmatrix} V_1 \\ V_2 \\ V_3 \end{pmatrix}; \begin{pmatrix} d_{nd} \\ d_{nq} \end{pmatrix} = [P(\theta)] \begin{pmatrix} d_{n1} \\ d_{n2} \\ d_{n3} \end{pmatrix}; \begin{pmatrix} I_d \\ I_q \end{pmatrix} = [P(\theta)] \begin{pmatrix} I_1 \\ I_2 \\ I_3 \end{pmatrix}$$

$[P(\theta)]$: Matrix Park

By applying the Park transformation to equation (22) and (23) we find the following relation

$$V_d = R_r I_d + L_r \frac{dI_d}{dt} + d_{nd} \cdot V_{dc} - L_r \omega I_q \quad (24)$$

$$V_q = R_r I_q + L_r \frac{dI_q}{dt} + d_{nq} \cdot V_{dc} + L_r \omega I_d$$

$$\frac{dV_{dc}}{dt} = \frac{1}{C_{dc}} [d_{nd} I_d + d_{nq} I_q]$$

The variables references values are defined to control. These are the reference voltages for the inverter.

$$V_d^* = V_d - U_d - e_q$$

$$V_q^* = V_q - U_q - e_d$$

With:

$$\begin{cases} U_d = R_r I_d + L_r \frac{dI_d}{dt} \\ U_q = R_r I_q + L_r \frac{dI_q}{dt} \end{cases} \text{ et } \begin{cases} e_d = -L_r \omega I_q \\ e_q = L_r \omega I_d \end{cases}$$

The general structure of the flow rotor orientation in a wind system is detailed in the figure below:

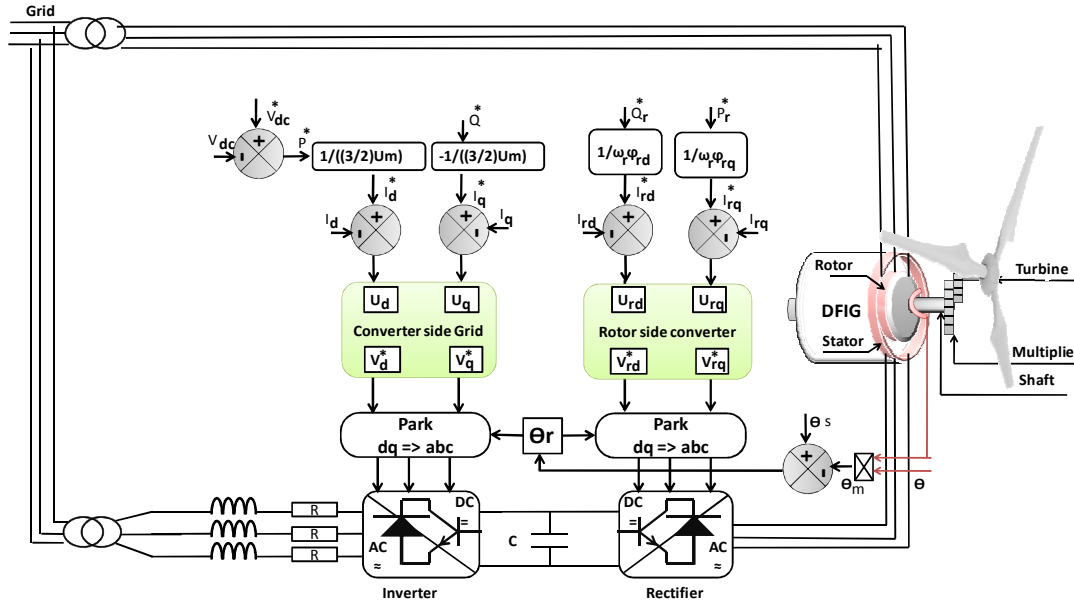


Figure 8. General structure of the orientation control the flow rotor applied to a wind system.

7 Simulation and Test Performance & Discussion

The following figure presents the global model of the wind system is simulated in the

Matlab/Simulink/. The model consists: the wind turbine, the doubly fed induction generator (DFIG), two power converters that connect the rotor to the grid:

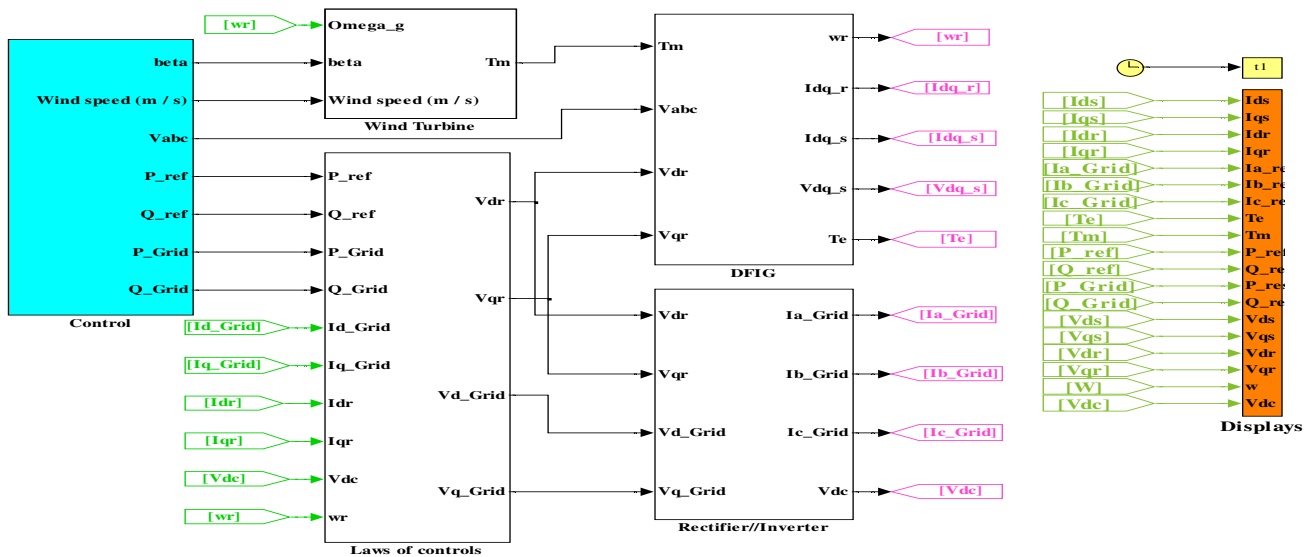


Figure 9. Simulation general diagram of the orientation control the flow rotor on Matlab / Simulink.

7.1 Response to Fixed Speed

The study made for a constant wind speed of $V=11\text{m/s}$. as shown in the following figure:

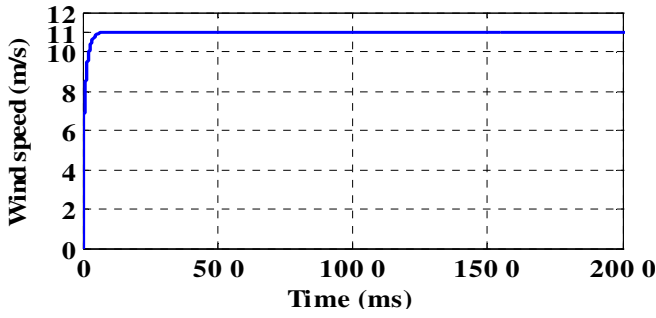


Figure 10. Wind Constant profile

The following figures show the wind system performance at constant speed.

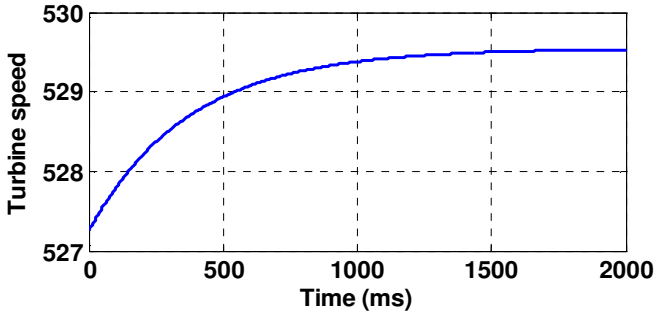
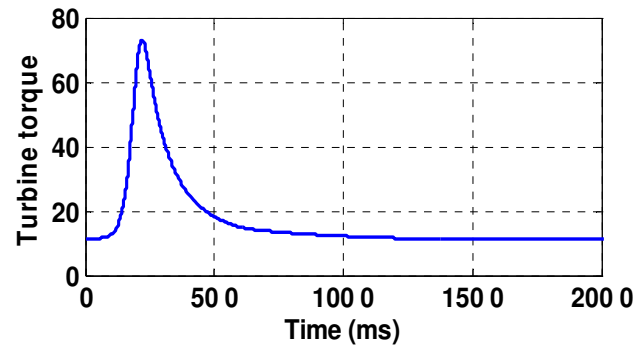
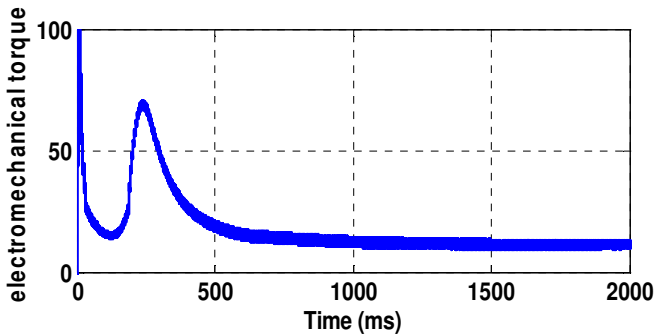


Figure 11. Turbine speed

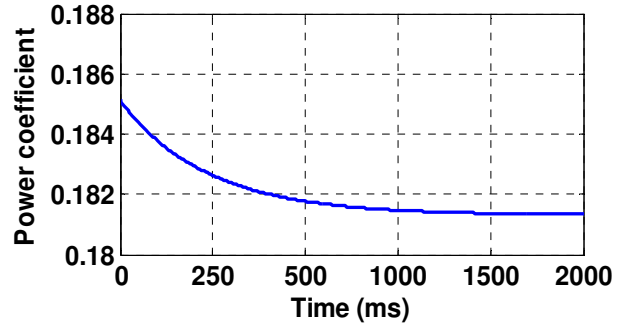


(a)

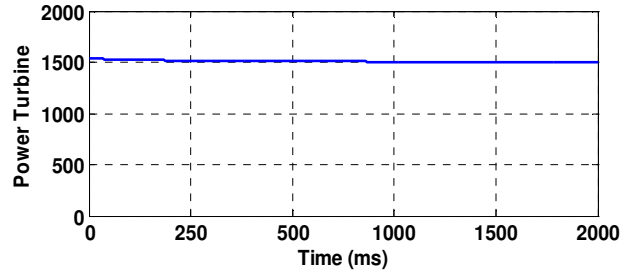


(b)

Figure 12. (a)Turbine torque, (b) electromechanical torque.

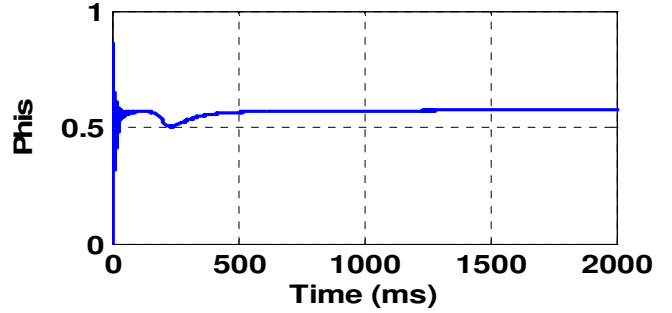


(a)

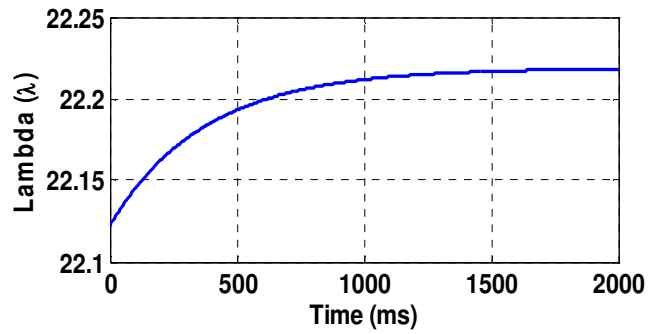


(b)

Figure 13. (a) Power coefficient, (b) Power turbine.

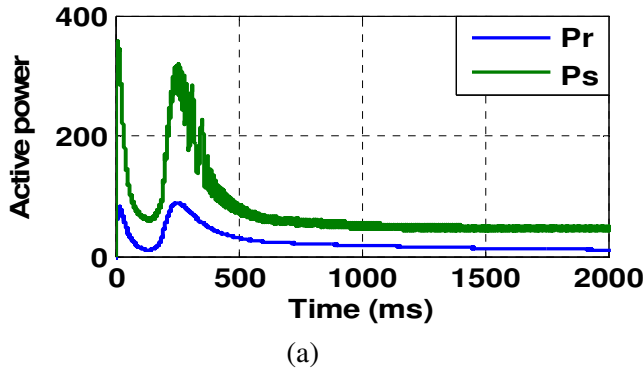


(a)

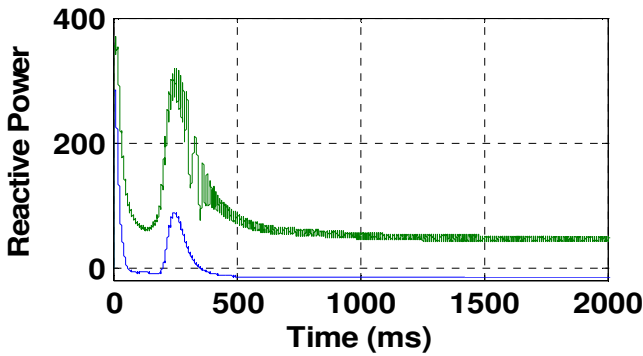


(b)

Figure 14. Characteristics of the turbine: (b) lambda, (a) Phis

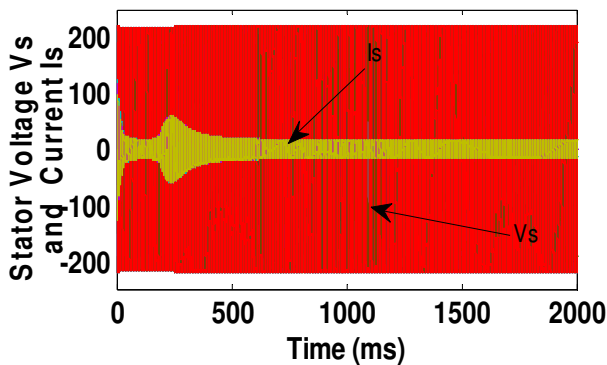


(a)

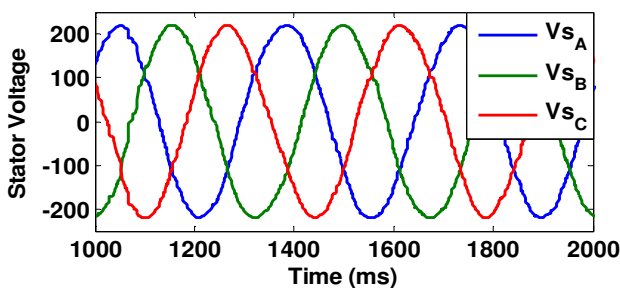


(b)

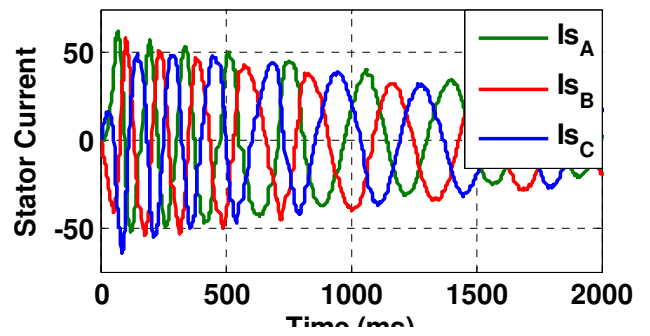
Figure 15. (a) The Power Active, (b) Power Reactive of MADA



(a)



(b)



(c)

Figure 16. (a) Stator voltage and current in the plan "abc" (b) Zoom stator voltage in the plan "abc", (c) Zoom stator current in the plan "abc".

It is observed that the grid currents are sinusoidal and in phase with the mains voltages, confirming that the inverter perfectly compensates the harmonic currents and the reactive power consumption on the one hand by the load and secondly the reactive power consumed by the DFIG. We also note that the frequency of the rotor currents is different from the frequency of the grid current. The DC bus voltage is perfectly maintained at its reference value to 1200V, as the rotor speed is regulated at 529.5 rad / s.

7.2 Response to a ramp

The wind system is supposed to functioning at its optimal point such as, at a wind speed $V=6$ m/s, the optimal specific speed $\lambda_{opt}=12$, the maximum power coefficient $C_p = 0.497$ and the wind extracts maximum performance by the MPPT method. At time $t = 0.5$ s the wind changes speed as a ramp to another value $V = 10$ m / s for a simulation time as shown in the following figure:

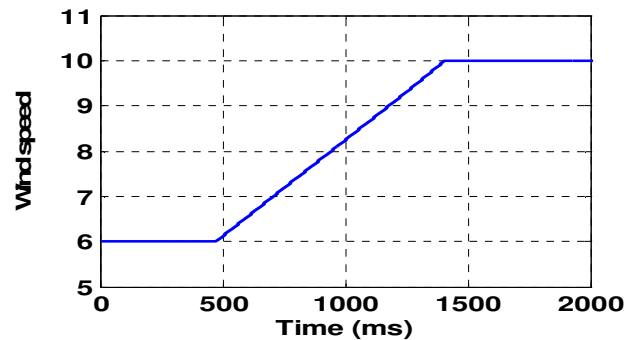


Figure 17. Evolution of the wind speed.

Following Figures present the results obtained for this application of the wind.

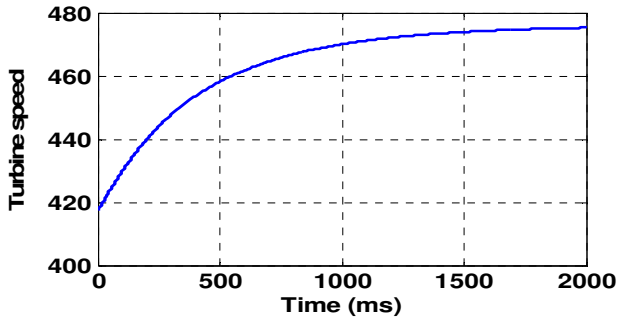
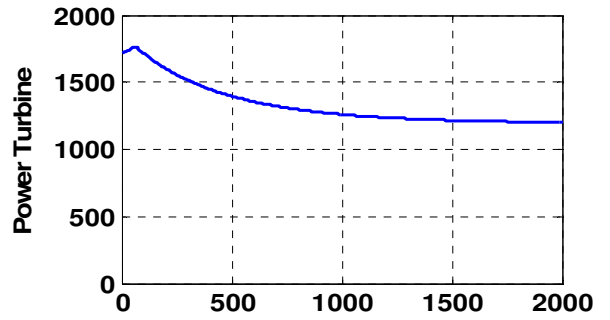
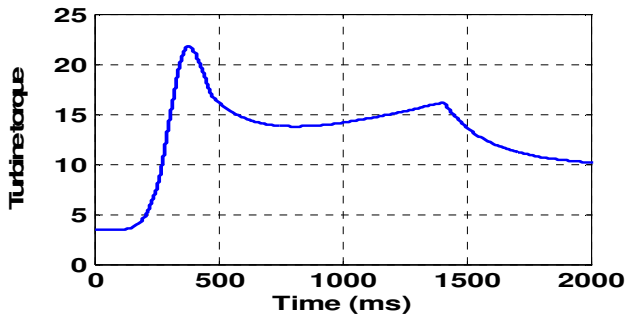


Figure 18. Turbine speed

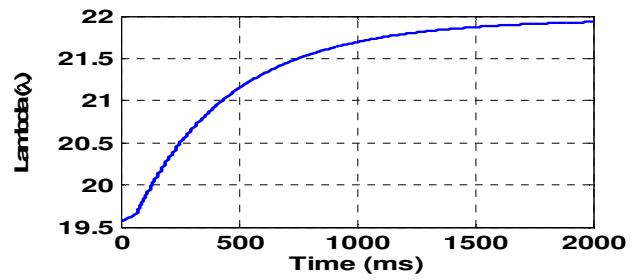


(b)

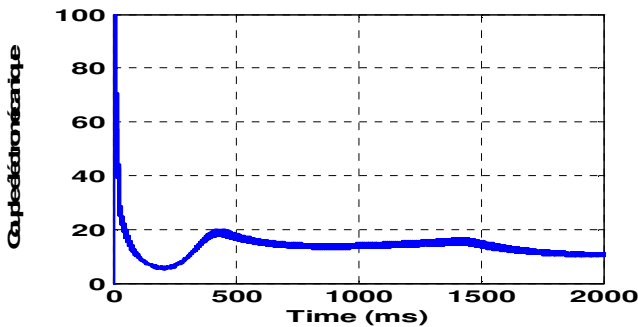
Figure 20. (a) Power coefficient, (b) Pwer turbine.



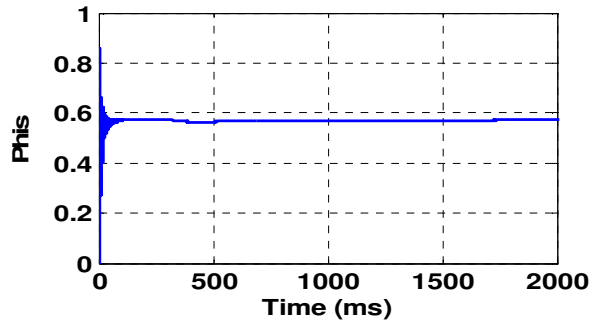
(a)



(a)



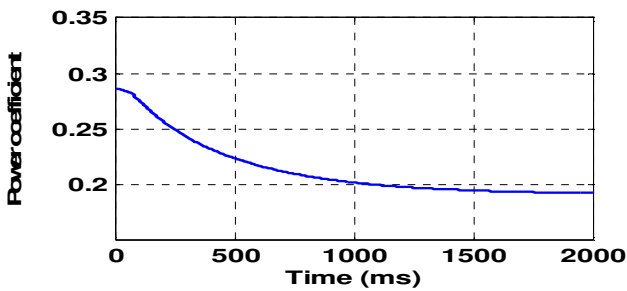
(b)



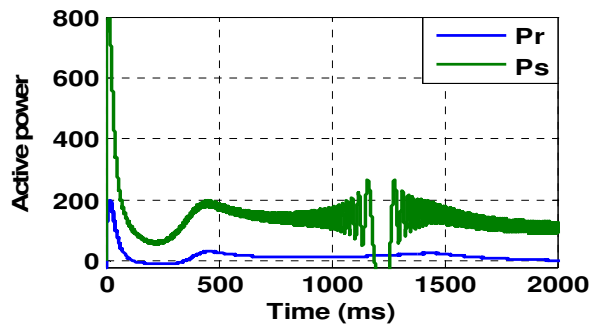
(b)

Figure 21. Characteristics of the turbine : (a) lambda, (b) Phis.

Figure 19. (a) Turbine torque, (b) Electromechanical Power



(a)



(a)

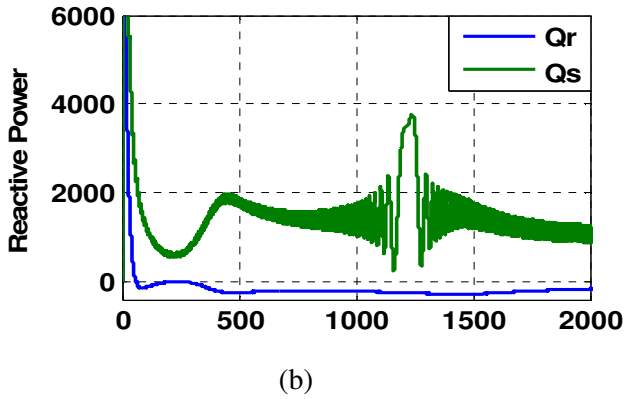
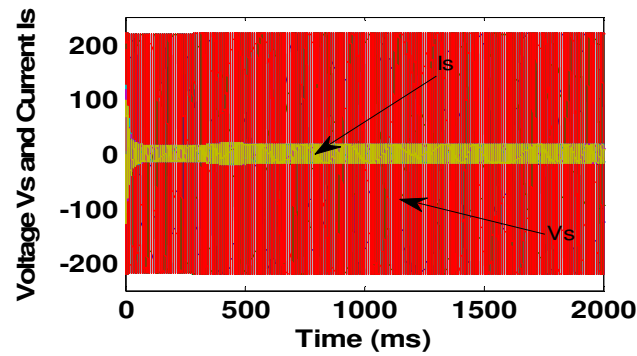
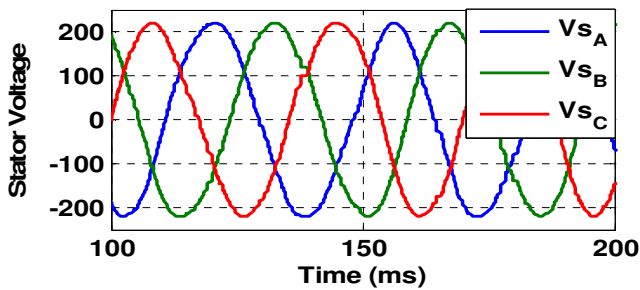


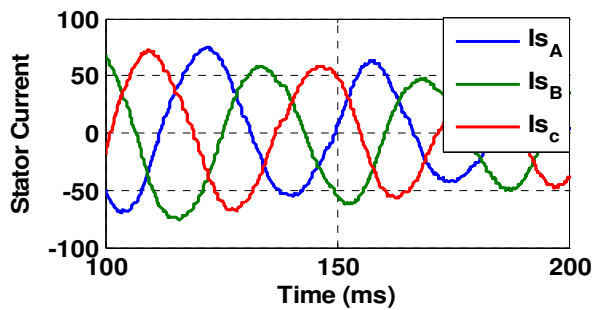
Figure 22. (a) Active Power, (b) Reactive Power of MADA



(a)



(b)



(c)

Figure 23. (a) Stator voltage and current in the plan "abc" (b) Zoom stator voltage in the plan "abc", (c) Zoom stator current in the plan "abc".

In the case of this wind model, note that the wind system practically functions the same manner previous, the active and reactive stator powers fluctuate and oscillating around their values in the case of the model. This phenomenon is due to the electronic switch at the rotor converter. From these simulations, One can notice the robustness of the vector control in terms of decoupling and the good results achieved by regulating the classical PI corrector which adequately ensured the wind MPPT system.

7.3 Response to variable speed

We applied a random wind profile closer to the evolution of the real wind was filtered to suit the dynamics of the system studied. The objective is to see the degree of maximum power point tracking and effectiveness of speed control provided by the conventional PI. The system parameters are given in the annexes. A random wind profile is applied to the system Figure 10.

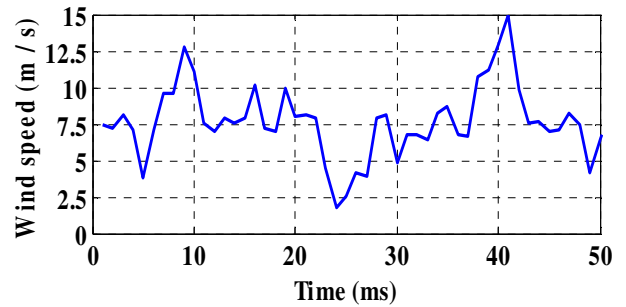
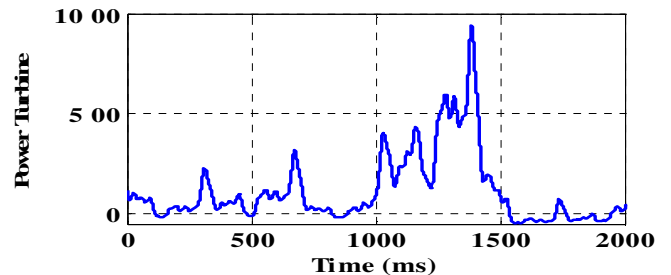


Figure 24. Profile of wind speed.

The following figures show the performance of the control system.



(a)

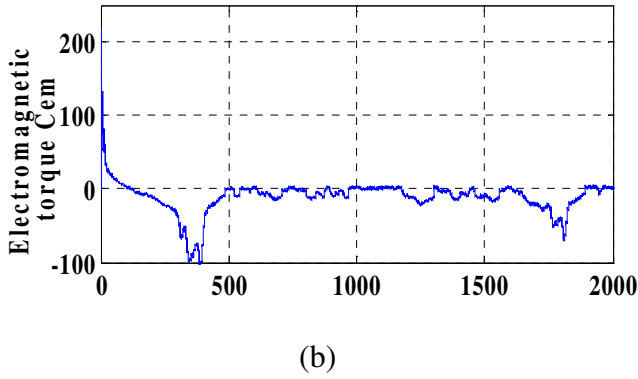


Figure 25. (a) Power of the turbine, (b) Electromagnetic torque.

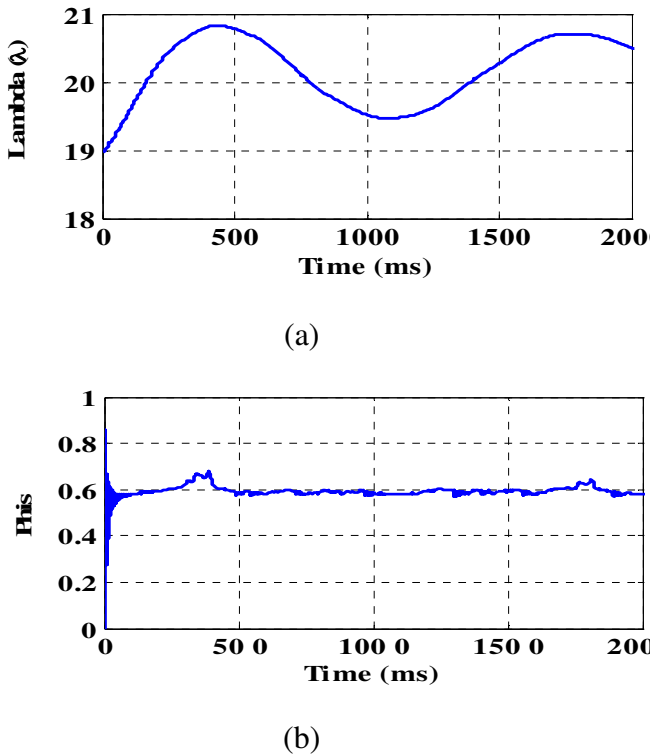


Figure 26. Characteristics of the turbine : (a) lambda, (b) phi_s.

The following two figures show the wave form of the active and reactive power, stator and rotor.

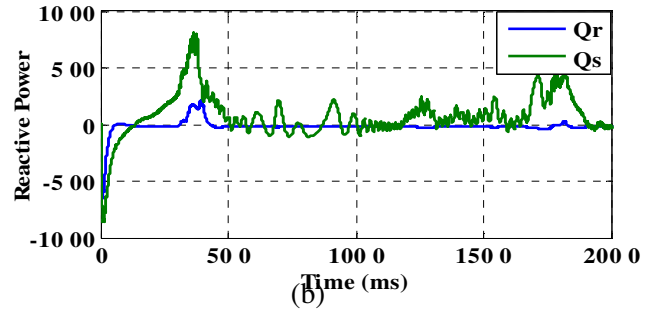
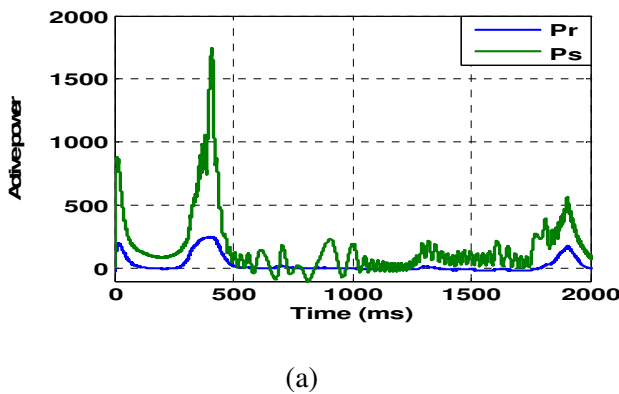


Figure 27. (a) The Power Active, (b) Power Reactive of MADA .

The following figure shows the wave forms of the voltages and stator currents.

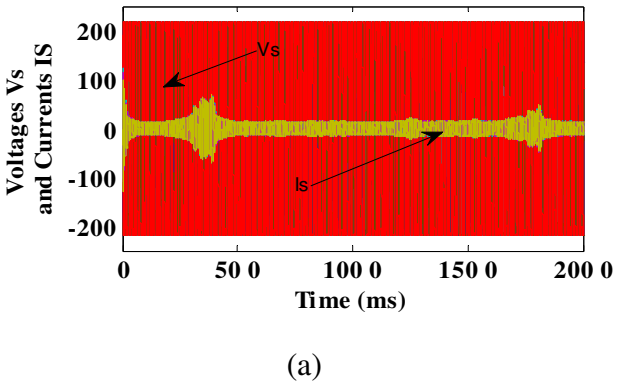


Figure 28. (a) Stator voltage and current in the plan "abc" (b) Zoom stator voltage in the plan "abc", (c) Zoom stator current in the plan "abc".

One can notice that the stator voltage is equal to that of the grid, while the currents obtained are sinusoidal, which implies a clean energy without harmonics supplied or drawn by the DFIG. The current and stator voltage are in phase opposition, this means that the stator active power is supplied from the generator to the grid.

8 Conclusion

The object of this work consists to control, analysis, development, modeling and simulation of a wind system operating at different wind speeds.

The application of the orientation control of the rotor flow as the direct axis "d" gives a simple stabilization of the wind system.

Indeed, it not only allows us to simplify the model of the machine but also to decouple torque control and the flow. From numerical simulation, it was found that effectively the rotor flow orientation technique to decouple the flow, the powers so that the direct component of the rotor current control reactive power and the quadrature component control the active power. This allows us to obtain high dynamic performance similar to that of the MCC. In this respect, this work can be continued and completed by the implementation of this command in a FPGA card.

Annex:

TABLE I. PARAMETERS OF WIND POWER SYSTEM

Parameters of the turbine	
Diameter of blade	R=35.25 m
Gain multiplier	G=16
Inertia of the turbine	J=0.3125 Kg.m ²
Coefficient of viscosity	f=0.00673 m.s ⁻¹
Parameters of the DFIG	
Stator resistance	Rs=0.455
Rotor resistance	Rr=0.62
Stator inductance	Ls=0.084H
Rotor inductance	Lr=0.081H
Mutual inductance	Msr=0.078H
Number of poles	P=2

References:

- [1] M.Taoussi, M.Karim, B.Bossoufi, A.Lagrioui, M.El Mahfoud, «The Fuzzy Control for Rotor Flux Orientation of the double-fed asynchronous generator Drive», *International Journal of Computers & Technology*, Mai 2013.
- [2] M.Taoussi, M.Karim, B.Bossoufi, D. Hammoumi, A.Lagrioui, "Speed Backstepping control of the double-fed induction machine drive", *Journal of Theoretical & Applied Information Technology*, Vol 74 Issue 2, pp 189-199, april 2015.
- [3] B.Bossoufi, M.Karim, A.Lagrioui, M.Taoussi, A.Derouich "Modeling and Backstepping Control of DFIG Generators for Wide-Range Variable-speed Wind Turbines" *Journal of Electrical Systems JES*, pp317-330. Vol.10 No.3, September 2014.
- [4] B.Bossoufi, M.Karim, A.Lagrioui, M.Taoussi, M.L.EL Hafyani "Backstepping control of DFIG Generators for Wide-Range Variable-Speed Wind Turbines" *IJAAC International Journal of Automation and Control*, Vol.8 No.2, pp 122-140, July 2014.
- [5] B.Bossoufi, M.Karim, A.Lagrioui, M.Taoussi, "FPGA-Based Implementation nonlinear backstepping control of a PMSM Drive" *IJPEDS International Journal of Power Electronics and Drive System*, Vol.4 No.1, pp 12-23, March 2014.
- [6] B.Bossoufi, M.Karim, A.Lagrioui, "Matlab & Simulink Simulation with FPGA-Based Implementation adaptative and not adaptative Backstepping nonlinear Control of a Permanent Magnet Synchronous Machine Drive" *WSEAS TRANSACTIONS on SYSTEMS and CONTROL*, pp86-100, Vol.9 No.1, February 2014.
- [7] B.Bossoufi, M.Karim, S.Ionita, A.Lagrioui, "Nonlinear Non Adaptive Backstepping with Sliding-Mode Torque Control Approach for PMSM Motor" *Journal of Journal of Electrical Systems JES*, pp236-248. Vol.8 No.2, June 2012.
- [8] B.Bossoufi, M.Karim, S.Ionita, A.Lagrioui, "Low-Speed Sensorless Control of PMSM Motor drive Using a NONLINEAR Approach BACKSTEPPING Control: FPGA-Based Implementation" *Journal of Theoretical and Applied Information Technology JATIT*, pp154-166, Vol. 36 No.1, 29th February 2012.
- [9] B.Bossoufi, M.Karim, S.Ionita, A.Lagrioui, "DTC CONTROL BASED ARTIFICIAL NEURAL NETWORK FOR HIGH

- PERFORMANCE PMSM DRIVE” *Journal of Theoretical and Applied Information Technology JATIT*, pp165-176, Vol. 33 No.2, 30th November 2011.
- [10] B. Bossoufi, M. Karim, S. Ionita, A. Lagrioui, “The Optimal Direct Torque Control of a PMSM drive: FPGA-Based Implementation with Matlab & Simulink Simulation” *Journal of Theoretical and Applied Information Technology JATIT*, pp63-72, Vol. 28 No.2, 30th June 2011.
- [11] Karim Belmokhtar, Mamadou Lamine Doumbia, “Modélisation et commande d’un système éolien à base de machine asynchrone à double alimentation pour la fourniture de puissances au réseau électrique” *Journal of Scientific Research*, Vol. 2, No 0, pp 54-62, Novembre 2010.
- [12] W. L. Kling and J. G. Slootweg, “Wind Turbines as Power Plants”. in *Proceeding of the IEEE/Cigré workshop on Wind Power and the impacts on Power Systems*, pp 17-18 June 2002, Oslo, Norway.
- [13] J. J. Chen and K. P. Chin, “Automatic flux-weakening control of permanent magnet synchronous motors using a reduced-order controller,” *IEEE Trans. Power Electron*, vol. 15, pp. 881-890, Sept. 2000.
- [14] M. Rodic, K. Jezernik, “Speed Senseless Sliding Mode Torque Control of Induction Motor”, *IEEE Trans on. Industrial Electronics*, February 2002.
- [15] Hisn-Jang Shieh and Kuo-Kai Shyu, “Non Linear Sliding Mode Torque Control With Adaptive Backstepping Approach For Induction Motor Drive”, *IEEE Transactions on Industrial Electronics*, Vol. 46, N° 2, April 1999, pp. 380-388.
- [16] Z. P. Jiang and H. Nijmeijer, “Tracking control of mobile robots: A case study in Backstepping,” *Automatica*, vol. 33, no. 7, pp. 1393–1399, Jul. 1997.
- [17] T. C. Lee, K. T. Song, C. H. Lee, and C. C. Teng, “Tracking control of unicycle-modeled mobile robots using a saturation feedback controller,” *IEEE Trans. Control Syst. Technol.*, vol. 9, no. 2, pp. 305–318, Mar. 2001.
- [18] T. H. Li, S. J. Chang, and Y. X. Chen, “Implementation of humanlike driving skills by autonomous fuzzy behavior control on an FPGA based car-like mobile robot,” *IEEE Trans. Ind. Electron.*, vol. 50, no. 5, pp. 867–880, Oct. 2003.
- [19] S. S. Solano, A. J. Cabrera, I. Baturone, F. J. Moreno-Velo, and M. Brox, “FPGA implementation of embedded fuzzy controllers for robotic applications,” *IEEE Trans. Ind. Electron.*, vol. 54, no. 4, pp. 1937–1945, Aug. 2007.
- [20] Y. F. Chan, M. Moallem, and W. Wang, “Design and implementation of modular FPGA-based PID controllers,” *IEEE Trans. Ind. Electron.*, vol. 54, no. 4, pp. 1898–1906, Aug. 2007.
- [21] S. H. Han, M. H. Lee, and R. R. Mohler, “Real-time implementation of a robust adaptive controller for a robotic manipulator based on digital signal processors,” *IEEE Trans. Syst., Man, Cybern. A, Syst., Humans*, vol. 29, no. 2, pp. 194–204, Mar. 1999.
- [22] D. Zhang and H. Li, “A stochastic-based FPGA controller for an induction motor drive with integrated neural network algorithms,” *IEEE Trans. Ind. Electron.*, vol. 55, no. 2, pp. 551–561, Feb. 2008.
- [23] C. F. Jung and C. H. Hsu, “Temperature control by chip implemented adaptive recurrent fuzzy controller designed by evolutionary algorithm” *IEEE Trans. Circuits Syst. I, Reg. Papers*, vol. 52, no. 11, pp. 2376–2384, Nov. 2005.
- [24] C. F. Jung and J. S. Chen, “Water bath temperature control by a recurrent fuzzy controller and its FPGA implementation,” *IEEE Trans. Ind. Electron.*, vol. 53, no. 3, pp. 941–949, Jun. 2006.